Diffractive, Regge-pole, and distorted-wave Born-approximation description of the $^{26}Mg(^{16}O, ^{14}C)^{28}Si_{g.s.}$ transition between 33 and 128 MeV*

C. K. Gelbke,† J. D. Garrett, M. J. LeVine, and C. E. Thorn
Brookhaven National Laboratory, Upton, New York 11973
(Received 30 June 1975; revised manuscript received 3 December 1975)

Angular distributions for the $^{26}Mg(^{16}O, ^{14}C)^{28}Si_{g.s.}$ transition have been measured at incident energies of 33 and 40 MeV using a magnetic spectrometer. These data together with previous measurements for this same transition at 45, 60, and 128 MeV incident energies have been analyzed in terms of a diffractive model, Regge-poles, and the distorted-wave Born approximation. The shapes of the angular distributions at all incident energies are reproduced in each of the three analyses. Parameters required to fit the diffractive and Regge-pole models to the data are compared to equivalent quantities extracted from the distorted-wave Born-approximation analysis, and the relevant parameters are found to be consistent in all three models. This agreement is due principally to the peripheral nature of these reactions. To simultaneously reproduce the angular shape at the lowest and highest energies in the distorted-wave Born-approximation analysis, it was necessary to assume an energy dependent absorption in the vicinity of the nuclear surface. The use of such potentials removes much of the energy dependence of the normalization between the predicted and measured cross sections.

NUCLEAR REACTIONS $^{26}Mg(^{16}O, ^{14}C)^{28}Si$; $E = 33$ and 40 MeV measured $\sigma(\theta)$; diffractive model, Regge pole, and DWBA analysis at $E = 33$, 40, 45, 60, and 128 MeV.

I. INTRODUCTION

A considerable quantity of heavy-ion-induced, few-nucleon transfer data is now available[1] for a variety of projectiles and targets. The range of incident energies for such data extends from below to well above the Coulomb barrier. Data for a specific transition, however, usually[2] do not exist for a wide range of incident energies. Angular distributions for the $^{26}Mg(^{16}O, ^{14}C)$ transition to the ground state of ^{28}Si are available at incident energies of 45 (Ref. 3), 60 (Refs. 3 and 4), and 128 (Ref. 5) MeV. This article presents new data for the $^{26}Mg(^{16}O, ^{14}C)^{28}Si_{g.s.}$ transition at 33 and 40 MeV incident energies.

The distorted-wave Born-approximation (DWBA) formalism is generally used for the analysis of heavy-ion-induced transfer data. It is informative, however, to apply diffractive[6-11] and Regge-pole[12-16] descriptions to the $^{26}Mg(^{16}O, ^{14}C)^{28}Si_{g.s.}$ transition, since experimental data exist for a wide range of incident energies (from 1.4 to 5.5 times the incident channel Coulomb barrier). For this transition, with $L = 0$ transfer and with the angular momentum in the incident and exit channels well matched, these simple descriptions with only three free parameters can successfully describe the details of the shape of the angular distributions as a function of energy. Parameters from the diffractive and Regge-pole descriptions also can

be compared to similar quantities extracted from an independent DWBA analysis of the data, providing insight into the connection between these models. Since the diffractive and Regge-pole formalisms applied in this study contain no nuclear structure information, they cannot be considered a complete description of the reaction. In particular, absolute cross sections cannot be obtained from these analyses, as is possible with the DWBA.

The new data are discussed in Sec. II; the DWBA, diffractive, and Regge-pole analyses are presented in Secs. III, IV, and V, respectively, and the conclusions are summarized in Sec. VI.

II. 33 AND 40 MeV DATA

The angular distributions corresponding to the $^{26}Mg(^{16}O, ^{14}C)$ transition to the ^{28}Si ground state measured at incident energies of 33 and 40 MeV were obtained using the ^{16}O beam of the Brookhaven National Laboratory (BNL) tandem facility. These data (shown in Fig. 1 together with the existing data at higher incident energies) were measured using a position sensitive silicon detector in the focal plane of the BNL quadrupole-dipole-dipole-dipole (QDDD) spectrometer.[17] Signals from the detector proportional to the energy and to the product of position and energy were sorted and displayed in a two-dimensional format using a Sigma 7 computer. Therefore, it was possible to distinguish the ^{14}C reaction products from other
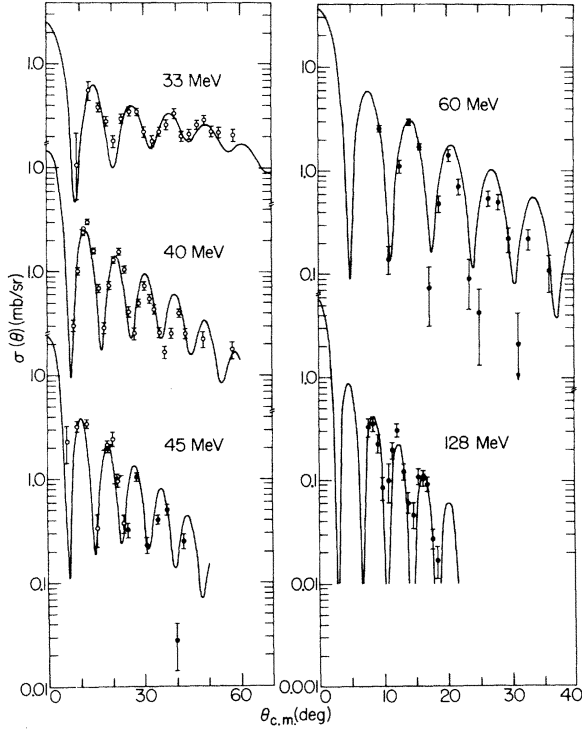
FIG. 1. Comparison of DWBA calculations and experimental cross sections for the ^{26}Mg(^{16}O, ^{14}C)^{28}Si$_{g.s.}$ transitions at 33, 40, 45, 60, and 128 MeV incident energies. The lowest two incident energies are from the present work and the 45, 60, and 128 MeV data is taken from Refs. 3–5, respectively. Data obtained using magnetic spectrometers are indicated by open circles. The spectroscopic amplitudes and the surface transparent optical potentials with an energy dependent surface absorption (Set 1) are given in Tables I and II, respectively. The calculated curves shown with the 33, 40, 45, and 60 MeV data are multiplied by 130, and the prediction shown with the 128 MeV data is normalized by a factor of 37. Note the change in the angular scale between the right and left portions of the figure.

particles with identical magnetic rigidity. The angular acceptance of the spectrometer was $\pm0.35°$. A Mg target of ≈65 $\mu g/cm^2$ thickness enriched to greater than 95% in ^{26}Mg and supported on a natural C backing of ≈20 $\mu g/cm^2$ thickness was used.

Relative cross sections were obtained by simultaneously measuring the ^{16}O elastic yield from ^{26}Mg in a fixed monitor detector. The absolute cross section scale was established by measuring the elastic scattering of ^{16}O on ^{26}Mg in the spectrometer at angles where the elastic scattering is expected to deviate from Rutherford by less than 1.5%. The distribution of charge states for the elastically scattered ^{16}O ions was measured in the spectrometer. Since these experimental values agree with the calculated[18] equilibrium charge state distribution, the published[18] values for both

O and C ions were used in obtaining absolute cross sections. An uncertainty of $\pm10\%$ is estimated for the absolute cross section scale. The vertical error bars shown with the 33 and 40 MeV data reflect only statistical uncertainties.

III. DWBA ANALYSIS

The DWBA cross section can be expressed as[19]

$$\frac{d\sigma}{d\Omega} = \frac{\mu_i \mu_f k_f}{(2\pi\hbar^2)^2 k_i} \frac{2J_B + 1}{(2J_A + 1)(2s_a + 1)} \sum_{LsjM} |\beta_{sj}^{LM}|^2 .$$

(1)

In the no-recoil limit[19] the reduced amplitudes are given by

$$\beta_{sj}^{LM} = \sum_{l_i l_f} i^{l_i - l_f - L} e^{i\sigma_i(l_i) + i\sigma_f(l_f)} I_{l_f l_i}^{Lsj} (2l_f + 1)^{1/2}$$

$$\times \langle l_f 0 L 0 | l_i 0 \rangle \langle l_f - M L M | l_i 0 \rangle Y_{l_f}^{-M}(\theta, 0) ,$$

(2)

where the z axis has been chosen along the direction of the incident beam. The initial and final channels are denoted by the indices i and f; L and M are the transferred orbital angular momentum and its projection. The radial integrals are given by

$$I_{l_f l_i}^{Lsj} = \frac{m_B}{m_A} \frac{4\pi}{k_i k_f} \int_0^\infty F_{Lsj}(r) f_{l_f}(k_f, \frac{m_A}{m_B} r) f_{l_i}(k_i, r) dr .$$

(3)

The remaining parameters are defined in the literature.[19]

In the present case, the ^{26}Mg(^{16}O, ^{14}C)^{28}Si ground state transition, $s = j = L = M = 0$, and the reduced amplitudes simplify to

$$\beta_{00} = \sum_l e^{i\sigma_i(l) + i\sigma_f(l)} I_{ll}^0 (2l + 1) P_l(\cos\theta)$$

$$= \sum_l e^{2i\delta_l} |I_{ll}^0| (2_l + 1) P_l(\cos\theta) .$$

(4)

The two-nucleon version[20] of the finite range code[21] RDRC was used to calculate the DWBA cross section. This code uses a microscopic form factor, but does not include the effects of recoil.

TABLE I. Two-nucleon spectroscopic amplitudes used in DWBA analysis.

^{16}O → ^{14}C [a]		^{26}Mg → ^{28}Si [a]	
$(1p_{1/2})^2$	0.88	$(1d_{5/2})^2$	1.03
$(1d_{5/2})^2$	−0.08	$(2s_{1/2})^2$	0.51
$(2s_{1/2})^2$	−0.11	$(1d_{3/2})^2$	0.25
$(1d_{3/2})^2$	−0.06		

[a] From Ref. 24.
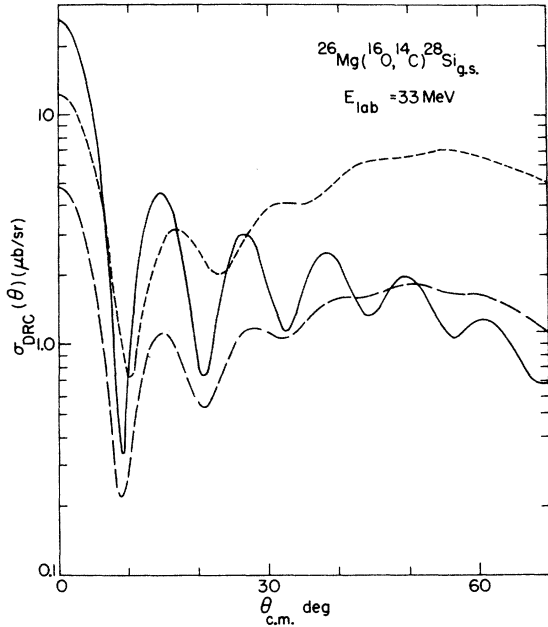
FIG. 2. Comparison of DWBA predictions for the ^{26}Mg(^{16}O, ^{14}C)^{28}Si$_{g.s.}$ transition at an incident energy of 33 MeV using three different optical potentials. The solid curve corresponds to calculations using surface transparent potentials (Set 1, Table II) and is shown with the experimental data in Fig. 1. The long and short dashed curves correspond to potential Sets 2 and 3, respectively, given in Table II. See text for discussion.

The DWBA analysis has been restricted to the no-recoil approximation, since investigations of the effects of recoil on single-nucleon transfer[22] and on two-nucleon transfer[23] have indicated that generally the magnitudes of the calculated cross sections are affected by the proper treatment of recoil and that the shapes of the angular distributions are only slightly changed. Since the diffractive and Regge-pole models contain no magnitude information, only the shapes of angular distributions are considered in the comparisons of the models with the DWBA, and therefore the simpler, no-recoil DWBA calculations have been used. The two-nucleon spectroscopic amplitudes of Nilsson et al.[24] (listed in Table I) were used in the calculation.

The angular shape of the predicted cross section at the lowest incident energy is particularly sensitive to the parametrization of the imaginary potential. Calculations with relatively weak absorption of Woods-Saxon geometry with a diffusivity ~0.5–0.6 fm do not reproduce the oscillating cross sections observed for an incident energy of 33 MeV (see the dashed curves in Fig. 2). Similar difficulties have been experienced[25-28] in reproducing other oscillating angular distributions at low bombarding energies, i.e., near the threshold for oscillating angular shapes. Attempts to reproduce the 33 MeV data by reducing the imaginary potential keeping a fixed Woods-Saxon geometry

TABLE II. Optical-model potentials used in the DWBA analysis

$$U(r) = V_c - V\frac{1}{1+e^x} - iW_{WS}\frac{1}{1+e^{x'}} + iW_{SD}4a'_{SD}\frac{d}{dr}\left(\frac{1}{1+e^{x''}}\right),$$

where

$$x = \frac{r-R}{a}, \quad x' = \frac{r-R'_{WS}}{a'_{WS}}, \quad x'' = \frac{r-R'_{SD}}{a'_{SD}}.$$

Channel and set	V (MeV)	R (fm)	$a = a'_{SD}$ (fm)	W_{WS} (MeV)	W_{SD} (MeV)	$R'_{WS}=R'_{SD}$ (fm)	a'_{WS} (fm)
			^{16}O + ^{26}Mg				
Set 1	100	6.69	0.50	65	a	6.40	0.05
Set 2	100	6.69	0.50	20	•••	6.69	0.50
Set 3 [b]	35	6.25	0.69	35	•••	5.70	0.61
			^{14}C + ^{28}Si				
Set 1	100	6.64	0.50	65	c	6.35	0.05
Set 2	100	6.64	0.50	20	•••	6.64	0.50
Set 3 [b]	35	6.21	0.69	35	•••	5.66	0.61
Bound state [d]	1.25 $A^{1/3}$		0.65	•••	•••	•••	•••

[a] $W_{SD}=0.54(E_{c.m.} - 18.58)$ MeV. Different values are shown for comparison in Fig. 4 and Table VII.

[b] Used for analysis of this same reaction at 45 MeV incident energy in Ref. 24.

[c] Same as for ^{16}O + ^{26}Mg channel.

[d] The bound state well depths were adjusted to give the individual transferred protons the proper binding energy.
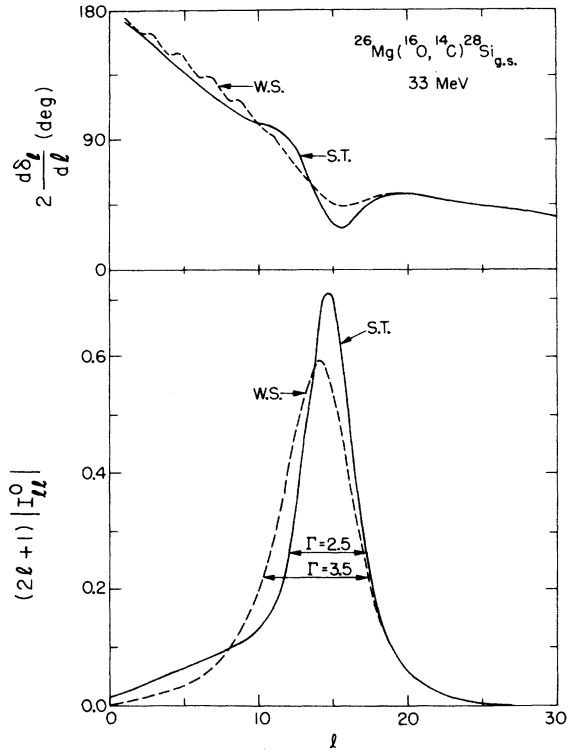
FIG. 3. Comparison of transfer amplitudes $(2 l_f + 1)|I^0_{l_i}|$ and phase derivatives $2 d\delta_l/dl$ calculated in the DWBA for the ^{26}Mg(^{16}O,^{14}C)^{28}Si ground state transition at 33 MeV incident energy using optical model Sets 1 (solid curves) and 2 (dashed curves) of Table II. All parameters in the two calculations are identical except for the form of the imaginary potential. The solid curve corresponds to surface transparent potentials, and the dashed curve was calculated using an imaginary potential with the same Woods-Saxon geometry as the real potential. The angular shapes of the differential cross sections corresponding to these two calculations are shown in Fig. 2.

have been unsuccessful. The solid curve in Fig. 2 was calculated with the same real potential as the long dashed curve, but with a surface transparent imaginary potential[29] (set 1, Table II). This curve reproduces the observed angular shape at 33 MeV (Fig. 1). Transfer amplitudes $(2l + 1)|I^0_{li}|$ and phase derivatives $2 d\delta_l/dl$ are compared in Fig. 3 for DWBA calculations (shown in Fig. 2) differing only in the imaginary potentials. The features of the surface transparent potentials which show a rapid change from weak absorption at the nuclear surface to strong absorption just inside the nucleus produce a better localized transfer amplitude and a more pronounced dip in the phase derivative than do weakly absorbing potentials of Woods-Saxon geometry. Both the better localization and the smaller magnitude of the phase derivative enhance the oscillations in the differential cross sections.[27,30,31] Indeed, oscillations are predicted using the surface transparent potentials, whereas the weakly absorbing potentials with identical real and imaginary Woods-Saxon geometry predict a grazing cross section except at the most forward angles (see Fig. 2).

If the optical model parameters are taken to be energy independent, the angular shapes can be reproduced for 33, 40, 45, and 60 MeV incident energies, but not for the 128 MeV data. The shape of the angular distribution obtained at 128 MeV, however, can be reproduced if the surface absorption W_{SD} is increased. The range of the surface absorption W_{SD} which (together with the parameters of set 1) allows a "reasonable fit" to the shape of the angular distribution, is given for each incident energy in Table III. The shapes of the 33 and 128 MeV angular distributions cannot be reproduced simultaneously using these parameters with any single value of W_{SD} (see Table III and Fig. 4).

TABLE III. Surface absorption and normalizations for DWBA analysis as described in text.

E_{lab} (MeV)	$E_{c.m.}$ (MeV)	W_{SD} (MeV) To fit shape [a]	$\sigma_{exp}(\theta)/\sigma_{DRC}(\theta)$	
			$W_{SD} = 1$ MeV [b]	Energy dep. W_{SD} [c]
33	20.43	≲2	130	130
40	24.76	≲4	100	130
45	27.86	≲8	90	130
60	37.14	≲10	65	130
128	79.24	≳5 [d]	e	37

[a] Range of surface absorption W_{SD} with parameter set 1, Table II to fit angular shape. See text.

[b] See Ref. 27 for fit to 33, 40, 45, and 60 MeV data.

[c] $W_{SD} = 0.54(E_{c.m.} -18.58)$ MeV used together with parameter set 1 of Table II. See Fig. 1 for fit with this normalization.

[d] Values as large as 100 MeV still reproduce the angular shape.

[e] Shape of 128 MeV angular distribution not reproduced for W_{SD} ≲5 MeV—see Fig. 4. $\sigma_{exp}(\theta)/\sigma_{DRC}(\theta) = 17$ for $W_{SD} = 5$ MeV.
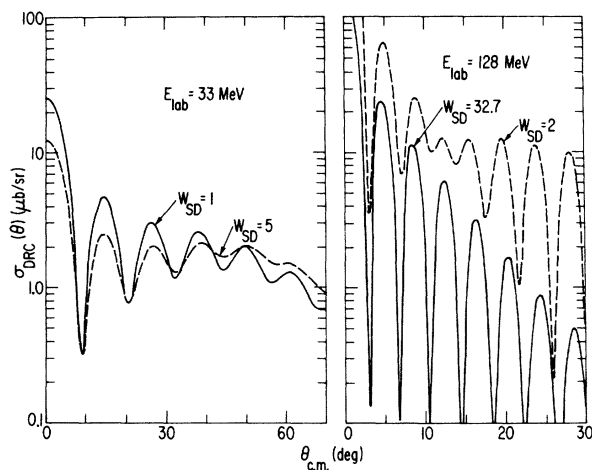
FIG. 4. Comparison of calculated DWBA cross sections (based on optical model parameter Set 1 of Table II) for the reaction $^{26}Mg(^{16}O,{}^{14}C)^{28}Si_{g.s.}$ at 33 and 128 MeV incident energy for a variation of the absorption W_{SD} in the region of the nuclear surface. The solid curves are calculated using the energy dependent absorption discussed in the text and are shown normalized to the experimental data in Fig. 1. A value of $W_{SD}=5$, which is about the lowest surface absorption to reproduce the 128 MeV data (see Table III), would not "fit" the 33 MeV data. Similarly, calculations using values of W_{SD} which reproduce the 33 MeV observed angular shape do not "fit" the 128 MeV data.

However, a good description of the data is obtained at all measured energies if the surface absorption is taken to be energy dependent. This is shown in Fig. 1, where the data are compared with calculations using the optical-model parameter Set 1 with a surface absorption of $W_{SD}=0.54\ (E_{c.m.}-18.58)$ MeV. Such an energy dependence accounts for the general features of the data between 33 and 128 MeV. However, it does not reproduce the details of the deep minima of the 45 and 60 MeV data quite as well as calculations based on a weaker surface absorption (see Fig. 17 of Ref. 27). A similar energy dependent absorption is required in such a potential parametrization to simultaneously reproduce the angular shapes of the $^{26}Mg(^{16}O,{}^{14}C)^{28}Si$ transitions at the lowest incident energies and the $^{26}Mg(^{16}O,{}^{15}N)^{27}Al$ transitions[4,32] at higher bombarding energies.

The present potential parameters have not been derived from an analysis of the elastic scattering data. Optical model calculations using these potential parameters are, therefore, not expected to reproduce the details of the elastic scattering angular distributions, especially at large scattering angles where $\sigma/\sigma_R < 0.1$. Whereas no elastic scattering data are available for the exit channel, elastic scattering data have been published at 45 and 60 MeV incident energies[32] for the entrance

channel. In Fig. 5 they are compared with optical model calculations utilizing the same potential parameters that have been used in the calculations of Fig. 1. The details of the elastic scattering measurements are not reproduced by these potentials which describe the energy dependence of the $^{26}Mg(^{16}O,{}^{14}C)^{28}Si$ transfer data. DWBA calculations using the recently published optical model parameters[32] obtained from a fit to the elastic data and such calculations based on potentials of the same geometry with reduced absorption do not predict the shapes of the $^{26}Mg(^{16}O,{}^{14}C)^{28}Si$ angular distributions at the lowest incident energies. Furthermore, it is noted that, at small scattering angles, single-nucleon transfer data induced by ^{16}O on ^{26}Mg also could not be reproduced by single-step DWBA calculations utilizing optical potential parameters derived from an analysis of elastic scattering data.[32] Similar difficulties have been encountered in the analysis of other heavy-ion-induced transfer reactions,[33] and very often surface transparent optical potentials had to be introduced.[28]

The energy dependence of the present potentials might be due to the neglect of second order effects which could be important in this reaction because of the rather large deformation of the target nucleus. Note that any neglect of coupled channel ef-
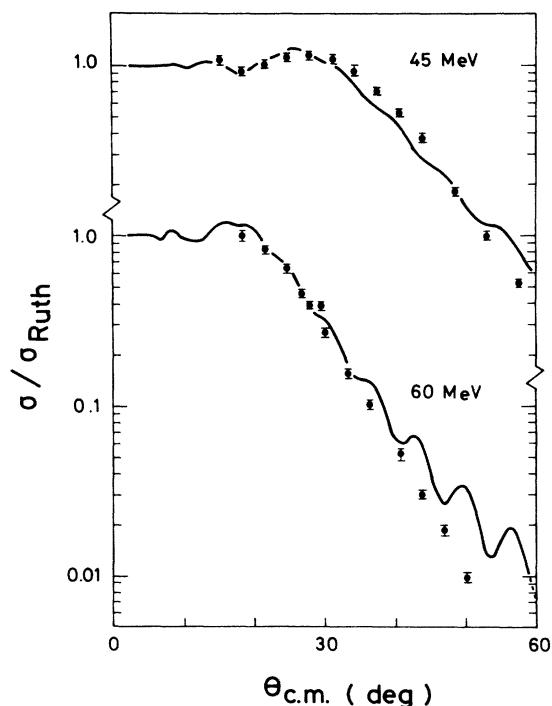
FIG. 5. Comparison of optical model calculations using the energy dependent surface absorption as in Fig. 1 to the entrance channel elastic scattering data at 45 and 60 MeV. The data have been taken from Ref. 32.
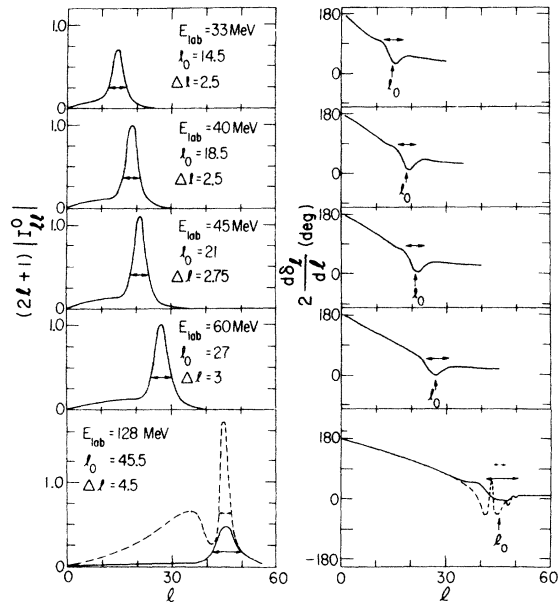
FIG. 6. Predicted transfer amplitudes $(2l_f+1)|I_{ll}^0|$ and phase derivatives $2d\delta_l/dl$ as a function of the final channel partial wave. Identical parameters to those used to calculate the differential cross sections shown with the $^{26}\mathrm{Mg}(^{16}\mathrm{O},\,^{14}\mathrm{C})^{28}\mathrm{Si}_{g.s.}$ experimental data in Fig. 1 were used. The $1/e$ full widths $2\Delta l$ are shown by the horizontal arrows with the phase derivatives. Also shown (dashed curve) for an incident energy of 128 MeV are values calculated with a weaker absorption near the nuclear surface—$W_{SD}=2$ MeV. The angular shape predicted for an incident energy of 128 MeV and $W_{SD}=2$ MeV is shown in Fig. 4. The anomalous disappearance of a sharp minima in the predicted cross section between 10 and 15° is the result of contributions from large amplitudes for the lower partial waves. In Fig. 7 the result of removing the contributions of the partial waves below $l=41$ is shown.

fects results in a modification of the imaginary potential.[19] A more complete analysis of the present reaction which includes a proper coupling between elastic and inelastic scattering as well as the dominating transfer channels would be necessary before deciding about the significance of the present energy dependence of the optical potential.

In order to see the effect of the energy dependence of the imaginary part of the optical potential, transfer amplitudes $(2l+1)|I_{ll}^0|$ and phase derivatives $\theta_l=2d\delta_l/dl$ corresponding to the DWBA calculations using the energy dependent surface absorption are plotted as a function of the exit channel partial wave l in Fig. 6. For comparison the values of the transfer amplitudes and phase derivatives calculated for 128 MeV incident energy using a weaker surface absorption $(W_{SD}=2\,\mathrm{MeV})$ are also shown as dashed curves in Fig. 6. For the case of weaker absorption at the nuclear surface, there

are contributions to the transition amplitude corresponding to small partial waves. Increasing the surface absorption essentially damps the contributions from these low partial waves. The anomalous angular shape calculated for the 128 MeV incident energy using the weaker surface absorption (see dashed curve in Fig. 4) is the result of interference between such contributions from the lower partial waves and those in the l window. When the lower partial waves are removed from the weak surface absorption calculation, oscillations are predicted in the 10–15° angular region (see Fig. 7).

Another effect of an increased absorption at the
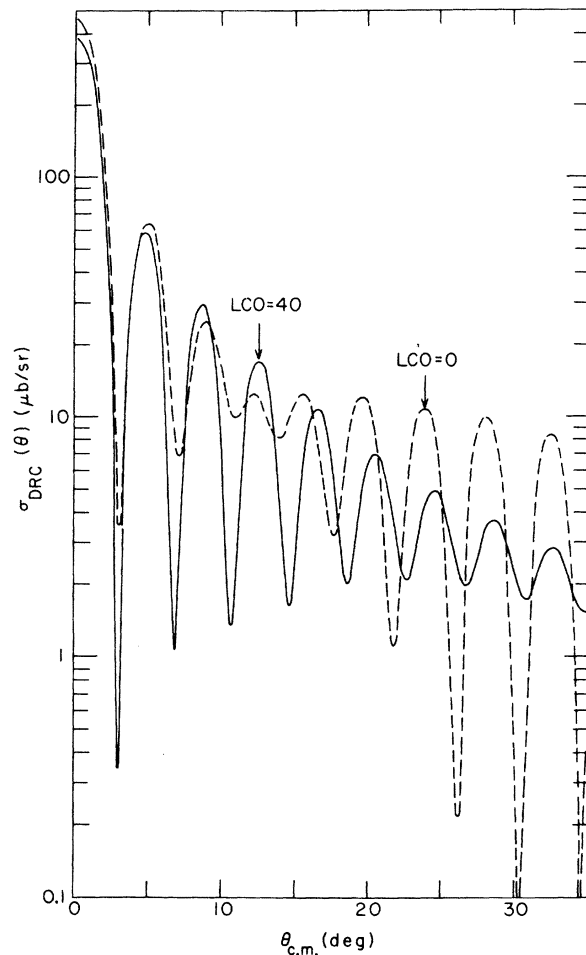
FIG. 7. Comparison of angular distribution predicted in the DWBA for the $^{26}\mathrm{Mg}(^{16}\mathrm{O},\,^{14}\mathrm{C})^{28}\mathrm{Si}$ ground-state transition at 128 MeV incident energy using optical model parameter Set 1 of Table II (solid curve) with $W_{SD}=2$ MeV with a calculation dashed curve with contributions of all partial waves <41 removed (see Fig. 6). The anomalous disappearance of sharp minima in the predicted cross section between 10 and 15° is apparently the result of contributions from the low partial waves.

nuclear surface is a smoother dependence of θ_l on angular momentum. In particular, the spike in θ_l which is observed for the weakly absorbing potentials near the grazing partial waves disappears for an increased absorption (see Fig. 6). Similar anomalous spikes in the phase derivative θ_l predicted for this transition at lower incident energies[27] also disappear when potentials with an increased surface absorption are used in the calculations.

The energy dependent surface absorption removes the variation of the normalization between calculated and experimental cross sections between 33 and 60 MeV incident energy (see Table III). The normalization of the 128 MeV data, however, is still a factor of ~3.5 less than that of the lower energy data. Perhaps this is not too surprising since the effects of recoil, which are neglected in the present calculation, would be expected to vary considerably between 60 and 128 MeV incident energies. Recoil also may account for part of the large factor (~130 for these calculations at the lower incident energy, see Table III) by which these calculations have to be normalized to reproduce the measured cross sections. Recent calculations[34] for (^{16}O, ^{14}C) reactions on ^{48}Ca and ^{208}Pb targets indicate that a very large basis of single-particle states can increase the predicted cross sections by a significant factor.

IV. DIFFRACTIVE DESCRIPTION

Various diffraction parametrizations which yield analytic expressions for the differential cross section[6-11] have been formulated. For the present case of $L = 0$ angular momentum transfer a very simple parametrization is used. This three-parameter prescription, which was first introduced by Strutinsky,[6] stresses the l-space localization about some critical angular momentum l_0. The reduced reaction amplitude is parametrized by approximating the phase by a linear function of angular momentum

$$\delta_l = \delta_{l_0} + \tfrac{1}{2}\theta_0(l - l_0) \tag{5}$$

and assuming a Gaussian distribution for the radial integrals (compare Eqs. 3 and 4)

$$\left|I_{ll}^0\right| = \eta_{l_0} \exp\left[-\left(\frac{l - l_0}{\Delta l}\right)^2\right]. \tag{6}$$

Here θ_0 may be interpreted as the classical scattering angle; l_0 is the critical angular momentum, and Δl is the width of the localization of the reaction amplitude in angular momentum space. Replacing the summation on l by an integration and using the asymptotic expression for the Legendre polynomials of large argument, one obtains

$$\frac{d\sigma}{d\Omega} \sim \frac{l_0 \Delta l^2 \eta_{l_0}^2}{2k^2 \sin\theta} \{ e^{-(\Delta l)^2(\theta_0 + \theta)^2/2} + e^{-(\Delta l)^2(\theta_0 - \theta)^2/2}$$

$$- 2e^{-(\Delta l)^2(\theta_0^2 + \theta^2)/2}$$

$$\times \cos[(2l_0 + 1)\theta + \pi/2]\}. \tag{7}$$

For $\theta_0 \Delta l \gg 1$ the interference term is negligible and a Gaussian angular distribution is obtained; it is localized at the scattering angle $\theta = \theta_0$ with the width $\Delta\theta = \sqrt{2}/\Delta l$. For $\theta_0 \Delta l \ll 1$ a strongly oscillating angular distribution is obtained.

The measured shapes of the ^{26}Mg(^{16}O, ^{14}C)^{28}Si$_{g.s.}$ angular distributions are well described by this diffractive parametrization. In Fig. 8 the data are compared to the predictions of the diffractive model with the three parameters l_0, Δ_l, and θ_0 chosen to give a minimum χ^2 at each incident energy. The values of the parameters and the minimum χ^2 values obtained are given in Table IV. As the figure and the tabulated χ^2 values show, the calculations fit the data quite well. However, the
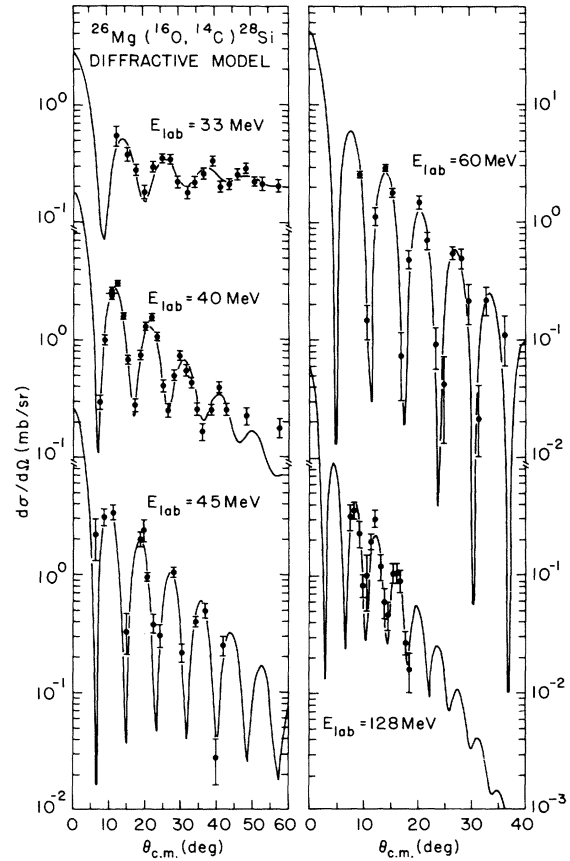
FIG. 8. Comparison of diffraction model calculations with the experimental data for the ^{26}Mg(^{16}O, ^{14}C)^{28}Si$_{g.s.}$ transition at 33, 40, 45, 60, and 128 MeV incident energies. See caption of Fig. 1 for data sources. The parameters used in the calculations are given in Table IV.

TABLE IV. Comparison of parameters used in the diffractive model analysis of the data (see Fig. 8) and corresponding values obtained from the DWBA analysis (see Fig. 6).

| E_{lab} (MeV) | Diffractive analysis | | | | DWBA analysis | | | |
	l_0 (Units of $\hbar$)	Δl (Units of $\hbar$)	θ_0 (deg)	χ^2	l_0 [a] (Units of $\hbar$)	Δl [a] (Units of $\hbar$)	θ_0 [b] (deg)	χ^2
33	14.9	2.70	52.1	1.7	14.5	2.5	44.6	3.8
40	17.9	2.59	20.9	4.8	18.5	2.5	26.0	20.3
45	20.7	2.13	10.5	3.1	21.0	2.75	16.9	14.3
60	27.4	3.35	0.0	3.3	27.0	3.0	11.3	12.0
128	46.2	5.44	6.9	1.1	45.5	4.5	−1.2	2.3

[a] Obtained from reaction amplitude of DWBA analysis (see Fig. 6).

[b] Average value of DWBA phase derivative in $l/e\ l$ window (see Fig. 6).

interpretation of the resulting parameters requires some caution. The parameter l_0 uniquely determines the period of oscillation of the angular distribution, which is well defined by the data at all energies, and the values of l_0 found in the diffractive analysis agree with those extracted from the DWBA (see Table IV). However, both θ_0 and Δl determine the amplitude of oscillation, the relevant quantity being roughly the product $\Delta l \theta_0$, so that neither parameter is uniquely determined. The data also do not define the amplitude of oscillation as precisely as they do the period. In particular, in the calculations no attempt was made to correct for the finite angular resolution of the data. In spite of these uncertainties, the values of Δl and θ_0 extracted from the DWBA agree qualitatively with the diffractive model (see Table IV). Indeed, at 33 MeV, where the amplitude of oscillation is best defined by the data, the product $\Delta l \theta_0$ is the same for both the DWBA and the diffractive analysis.

By assuming Rutherford trajectories for the particles and that the reaction takes place at the distance of closest approach R_c the l-space localization demonstrated in the DWBA and diffractive analyses may be transformed into an R-space

localization ΔR_c by

$$R_c = k^{-1}\{\eta + [\eta^2 + l_0(l_0 + 1)]^{1/2}\} \tag{8}$$

and

$$\Delta R_c = \left(\frac{E_{c.m.}/E_{CB} - 1}{2E_{c.m.}/E_{CB} - 1}\right)R_c\frac{\Delta l}{l_0}. \tag{9}$$

Here η is the Coulomb parameter of the reaction $\eta = Z_1 Z_2 e^2 m/\hbar^2 k$, $E_{c.m.}$ is the center of mass energy, and E_{CB} is the Coulomb energy at the distance R_c.

The distance of closest approach R_c, the width of the R-space localization ΔR_c, and the asymptotic wave length λ for the relative motion of the particles in entrance and exit channels calculated using these formulas and the values of Δl and l_0 taken from the DWBA analysis (Table IV) are collected in Table V.

Two points should be noted: (i) The reaction appears to be localized at a distance of closest approach around 9.1 ± 0.6 fm. Due to the neglect of the attractive nuclear interaction this value is expected to be an upper limit. (ii) The reaction appears to be extremely well localized independent of the incident energy. The width of the R-space localization, however, is much smaller than the

TABLE V. Distance of closest approach in R-space localization assuming Rutherford trajectories.

| E_{lab} (MeV) | Incident channel | | | | | Exit channel | | | |
	$E_{c.m.}$ (MeV)	η	R_c [a] (fm)	ΔR_c [a] (fm)	λ (fm)	$E_{c.m.}$ (MeV)	η	R_c [a] (fm)	ΔR_c [a] (fm)	λ (fm)
33	20.43	10.50	9.3	0.34	2.03	17.95	9.51	9.7	0.39	2.23
40	24.76	9.53	9.0	0.35	1.84	22.28	8.54	9.3	0.38	2.00
45	27.86	8.99	8.9	0.35	1.74	25.35	8.00	9.2	0.39	1.87
60	37.14	7.78	8.7	0.35	1.50	34.66	6.84	9.0	0.37	1.60
128	79.24	5.33	8.5	0.38	1.03	76.76	4.60	8.7	0.39	1.08

[a] Calculated using Eqs. (8) and (9) with l_0 and Δl from the DWBA reaction amplitudes shown in Fig. 6 and listed in Table IV. Identical values of l_0 and Δl have been used in both the incident and exit channels. This is reasonable because the reaction in "well matched" in l space — otherwise such simple diffractive and Regge-pole analyses probably would not reproduce the angular shapes.

σ vs R_{co}

33 MeV

60 MeV

128 MeV

REAL NUCLEAR
+ COULOMB
POTENTIAL

σ_{DRC} (μb)

POTENTIAL ENERGY (MeV)

R (fm)
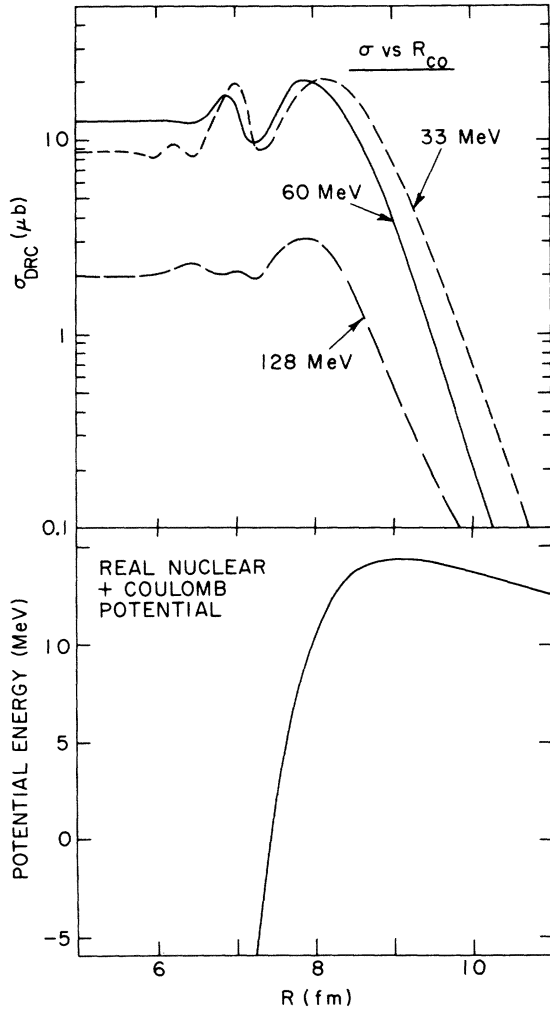
FIG. 9. Predicted total cross section for the ^{26}Mg-$(^{16}$O,^{14}C$)^{28}$Si$_{g.s.}$ transition at 60 MeV as a function of a lower cutoff on the radial integration. Optical model parameter Set 1 of Table II was used in the calculations. The variation of total cross section between 6.5 and 8 fm results from removing contributions which cause cancellations in the cross sections. The rapid decrease in total cross sections for cutoffs greater than 8 fm demonstrates that the main transfer contribution is obtained (see Ref. 37) at such radial distances. In the lower portion of the figure the sum of the real nuclear plus Coulomb potential for the ^{16}O+^{26}Mg channel is shown as a function of radii for comparison.

wave length of relative motion, indicating that the connection between l-space localization and R-space localization should not be taken too seriously. It has been pointed out[35,36] that the localization of the reaction amplitudes in l space mostly is the result of phase averaging and only to some extent is due to the localization of the overlap of the wave functions in the initial and final states.

For comparison, the radial dependence of the

calculated DWBA total cross section is shown in Fig. 9 as a function of lower cutoffs in the radial integration.[37] The sum of the real nuclear (optical model parameter set 1 of Table II) plus Coulomb potential in the entrance channel also is shown as a function of the radius. The main contribution to the calculated DWBA cross section is associated with radii of $9.3^{+0.6}_{-0.3}$ fm for 33 MeV incident energy.[38] The radial region contributing to the DWBA cross section has decreased to $\sim 8.8^{+0.6}_{-0.3}$ fm for 60 MeV incident energy and remains nearly constant up to an incident energy of 128 MeV. This latter value is slightly less than the average distance of closest approach in entrance and exit channels obtained by assuming Rutherford trajectories (see Table VI). In a classical picture the difference of the two distances may be explained as the attraction of the nuclear potential which is taken into account in the DWBA calculations but not by assuming Rutherford trajectories. The dominant contributions to the ^{26}Mg$(^{16}$O, ^{14}C$)^{28}$Si reaction at energies sufficiently above the Coulomb barrier are apparently associated with radii near the Rutherford or interaction radius (i.e., the radius at which the real nuclear and Coulomb forces balance—see Fig. 9). A similar lower radial cutoff analysis of the DWBA cross section indicates that contributions to heavy-ion-induced single-nucleon transfer also is peaked near the Rutherford radius.[27]

V. REGGE-POLE ANALYSIS

The Regge-pole analysis of heavy-ion transfer data described in Ref. 14 assumes that the wave function in the scattering channels may be approximated to a good degree of accuracy by a single pole contribution. This has, in fact, been demonstrated to be true for several cases.[12-16] Such a description is based on the following ansatz for the wave function in the entrance channel[14]:

$$\psi_\alpha^{(+)}(\vec{k}_i, \vec{r}_i) = f_\alpha(r_i)g_\alpha(\hat{k}_i, \hat{r}_i). \tag{10}$$

The angular dependence of the wave function is given by

$$g_\alpha(\hat{k}_i\hat{r}_i) = \sum_{l_i m_i} \frac{\exp[i(\frac{1}{2}\pi)l_i + i\sigma_i(l_i) + i\delta'_i l_i]}{(l_i - \alpha)(l_i + \alpha + 1)}$$

$$\times Y^*_{l_i m_i}(\hat{k}_i)Y_{l_i m_i}(\hat{r}_i). \tag{11}$$

The wave function in the exit channel is obtained from the relation[19]

$$\chi^{(-)}(\vec{k}, \vec{r})^* = \chi^{(+)}(-\vec{k}, \vec{r}), \tag{12}$$

giving

$$\psi_\beta^{(-)}(\vec{k}_f, \vec{r}_f)^* = f_\beta(r_f)\bar{g}_\beta(\hat{k}_f, \hat{r}_f) \tag{13}$$

with

TABLE VI. Interaction radius summary.

Interaction radius (fm) \ E_{lab} (MeV)	33	40	45	60	128
A. Coulomb trajectory transformation of l-space localization to R space [a]					
Incident channel	9.3	9.0	8.9	8.7	8.5
Exit channel	9.7	9.3	9.2	9.0	8.7
B. Radial cutoff on DWBA calculations [b]					
$R_{1/2}$ [c]	9.25	8.80	8.75		
$R_{90\%} - \sigma_{10\%}$ [d]	9.0–9.9	8.5–9.4	8.5–9.4		
C. Rotational energy of "quasimolecular state" [e]					
Incident channel	$R_{rot} = 8.3$ fm				
Exit channel	$R_{rot} = 8.6$ fm				

[a] See Table V.

[b] See Fig. 9.

[c] Lower radial cutoff radius where R_{total} is half the value of that calculated with no cutoff (see Fig. 9).

[d] Range of lower radial cutoff radii where σ_{total} is between 90% and 10% of the value calculated with no cutoff in the radial integration (see Fig. 9).

[e] See discussion in Sec. V of text.

$$\bar{g}_\beta(\hat{k}_f, \hat{r}_f) = \sum_{l_f m_f} \frac{\exp[-i(\frac{1}{2}\pi)l_f + i\sigma_f(l_f) + i\delta'_f l_f]}{(l_f - \beta)(l_f + \beta + 1)} Y^*_{l_f m_f}(\hat{k}_f) Y_{l_f m_f}(\hat{r}_f) .$$ (14)

The asymptotic wave vector is denoted by $\vec{k}$ and the Coulomb phase shift by σ. The additional phase shift due to the nuclear potential is approximated by a linear function of angular momentum, the slope of which is the parameter δ'. The Regge poles in the entrance and exit channels are given by the complex numbers α and β, respectively.

In the no-recoil approximation the reduced transfer amplitude then is given by

$$\beta_{LM} = C_{LM} \sum_{l_i l_f} \frac{\exp[\frac{1}{2}i\pi(l_i - l_f) + i\sigma_i(l_i) + i\sigma_f(l_f) + i\delta'_i l_i + i\delta'_f l_f]}{(l_i - \alpha)(l_i + \alpha + 1)(l_f - \beta)(l_f + \beta + 1)} \langle l_f 0 L 0 | l_i 0\rangle\langle l_f - M L M | l_i 0\rangle(2l_f + 1)^{1/2} Y_{l_f}^{-M}(\theta, 0) ,$$ (15)

and is related to the transfer cross section by Eq. (1). Nuclear structure effects enter only via the radial form factor through the normalization constants C_{LM}. If the angular momentum transfer is uniquely determined, the shape of the angular distribution is independent of the specific structure of the states involved. In the present case, the angular momentum transfer is $L = 0$. The number of free parameters is reduced by assuming identical poles and nuclear phase shifts in the initial and final channels, i.e., $\alpha = \beta$ and $\delta'_i = \delta'_f = \delta'$. Such an assumption, justified a posteriori by the ability to reproduce the experimental data (see also Refs. 14–16), is possible because the incident and exit channel angular momenta are quite well matched. Thus Eq. (15) reduces to the simple expression

$$\beta_{00} = C_{00} \frac{1}{\sqrt{4\pi}} \sum_l \frac{\exp[i\sigma_i(l) + i\sigma_f(l) + 2\delta' l]}{(l - \alpha)^2(l + \alpha + 1)^2}$$

$$\times (2l + 1)P_l(\cos\theta)$$ (16)

$$\equiv C_{00} \frac{1}{\sqrt{4\pi}} \sum_l e^{2i\delta_l}(2l + 1)I^0_{ll}P_l(\cos\theta) .$$

As in the case of the diffractive model, the shape of the angular distribution is described by three parameters: the real and imaginary parts of the pole α and the slope of the nuclear part of the phase shift δ'. Figure 10 demonstrates that the shapes of the angular distributions at all energies are satisfactorily described by the Regge-pole analysis. The curves shown in the figure represent a best fit to the data obtained by varying Reα, Imα, δ', and the magnitude of the calculated
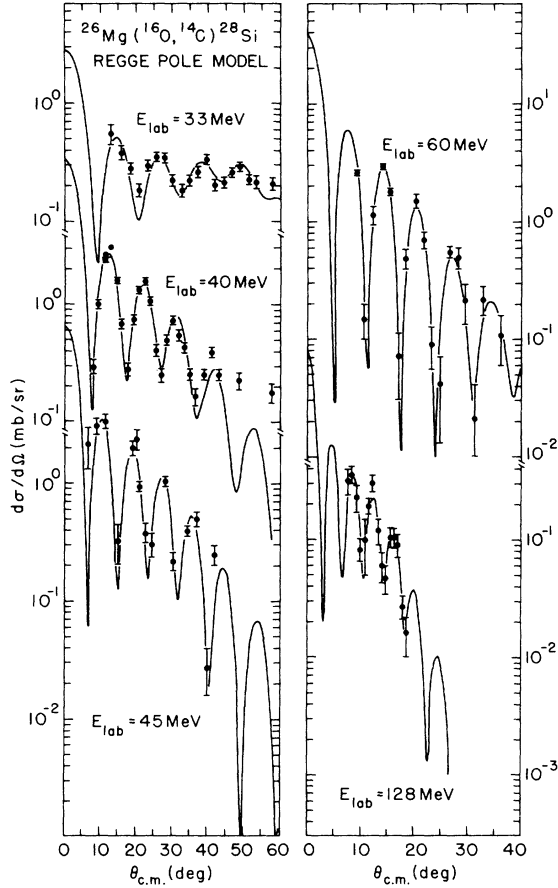
FIG. 10. Comparison of Regge-pole calculations with experimental data for the $^{26}\text{Mg}(^{16}\text{O},^{14}\text{C})^{28}\text{Si}_{\text{g.s.}}$ transition at 30, 40, 45, 60, and 128 MeV incident energy. See caption of Fig. 1 for data sources. The calculations are described in the text and the parameters used are contained in Table VII.

differential cross section. The final parameters and resulting χ^2 values are listed in Table VII.

The Regge-pole and diffractive prescriptions both fit the data equally well, as a comparison of Figs. 8 and 10 and the χ^2 values in Tables IV and VII show. Also, the parameters l_0 and Reα are nearly identical at each energy and Δl and Imα are similar, both showing a gradual increase with energy. This is to be expected, since a comparison of the two models shows the l-space distributions of transfer amplitudes to be similar in shape to each other and to the DWBA.

The main differences between the diffraction and Regge descriptions is that the former assumes a Gaussian and the latter essentially a Lorentzian distribution of the amplitudes I^0_{ll} [compare Eqs. (6) and (16)]. In order to see how sensitively angular distributions depend on the details of the various analyses it is instructive to compare them with the DWBA calculations. This has been done by

fitting the DWBA calculations with the diffraction and Regge descriptions. Table VIII gives the best fit parameters. Figure 11 compares the magnitudes of the radial integrals $|I^0_{ll}|$, and the phase derivatives $\theta_l = 2d\delta_l/dl$, for both the diffractive, Regge-pole, and DWBA descriptions at 33 and 60 MeV incident energies. The corresponding angular distributions are compared in Fig. 12. Again, the parameters which determine the peak of the l-space distribution of amplitudes, l_0 and Reα, are well determined and nearly equal for both models. The widths of the distributions, measured by Δl and Imα, also are very similar for the two models and for the DWBA (see Fig. 11). The values of phase parameters in the two models θ_0 and δ' are not so simply related, although Fig. 11 suggests that the parameter θ_0 of the diffractive model represents some average value of the (nonconstant) phase derivative in the l window.

The parameters of the Regge and diffraction models may be related to each other by requiring that the positions of the maxima and the widths at half maximum of the radial integrals $|I^0_{ll}|$ be the same and that the values of the phase derivatives θ_l in the l window be similar. This yields the relations

$$l_0 = \text{Re}\alpha , \tag{17}$$

$$\Delta l = 1.20 \text{Im}\alpha , \tag{18}$$

$$\theta_0 \approx 2\tan^{-1}\left(\frac{\eta}{\text{Re}\alpha}\right) + 2\delta' - \frac{2}{\text{Im}\alpha} . \tag{19}$$

Comparing the best fit parameters given in Table VIII, one obtains good agreement with the relations (17) and (18). However, the values of θ_0 are generally larger than expected from Eq. (19) by about 20°. Therefore, the values of θ_0 used in the diffraction model represent an average of the phase derivatives over the entire l window and are not determined by the minimum values at $l = l_0$ as is implied in Eq. (19). It already has been pointed out that smaller values of both the phase derivative and the width of the l-space window produce stronger oscillations in the angular distribution. If the product (Imα)δ' (or $\Delta l\theta_0$) is kept constant, χ^2 changes very little for large changes

TABLE VII. Best fit Regge parameters from analysis of data (see Fig. 10).

E (MeV)	Reα	Imα	δ' (rad)	χ^2
33	14.9	2.31	0.116	3.1
40	17.9	2.48	−0.009	6.5
45	20.7	2.12	0.063	3.2
60	27.5	2.30	0.026	1.7
128	46.3	5.18	0.095	0.8

TABLE VIII. Parameters resulting from fit of Regge and diffractive models to DWBA cross section.

		Regge model					
		Best fit [a]		Imα = 2.26 [b]		Imα = 0.113 Reα [b]	
E (MeV)	Reα	Imα	δ' (rad)	δ' (rad)	χ^2/χ^2_{min}	δ' (rad)	χ^2/χ^2_{min}
33	14.7	2.19	0.103	0.082	4.2	0.319	7.9
40	18.7	1.98	0.125	0.079	3.3	0.103	1.6
45	21.2	1.95	0.122	0.089	1.1	0.074	1.2
60	27.4	2.19	0.118	0.130	2.2	0.064	6.8
128	46.3	2.95	0.075	0.080	3.1	0.056	8.7

		Diffractive model					
		Best fit [a]		Δl = 2.47 [c]		Δl = 0.124l_0 [c]	
E (MeV)	l_0	Δl	θ_0 (deg)	θ_0 (deg)	χ^2/χ^2_{min}	θ_0 (deg)	χ^2/χ^2_{min}
33	14.6	1.82	55.3	39.9	4.3	55.8	1.0
40	18.7	2.09	32.9	29.3	1.3	31.0	1.1
45	21.2	2.18	25.5	25.8	1.1	23.7	1.1
60	27.3	2.54	15.3	14.8	1.0	16.0	2.7
128	46.4	3.08	3.95	−10.3	4.8	16.8	3.6

[a] Three parameter best fit.
[b] Fit constraining Imα as described.
[c] Fit constraining Δl as described.

in Imα (or Δl). Hence the values of Imα (or Δl) are not very well defined and it is possible to obtain reasonable fits to the DWBA calculations either by using energy independent values of Imα (or Δl) or by keeping the ratio Imα/Reα (or $\Delta l/l$) constant with energy (see Table VIII and Fig. 12).

The nonlinearity of the phase derivative in the l window seems to have only a subtle influence on the shape of the angular distribution. For the DWBA and for the Regge calculations θ_l has a minimum in the l window at all energies (see Fig. 6). The consequence of such a behavior of the phase is a predicted[15,39] modulation of the amplitude of the oscillations. That only the details of the amplitude of oscillation and not their general appearance are affected is clear from the fact that the angular shapes observed in the present study are as well described by the diffractive (without the phase dip) as by the Regge-pole (with the phase dip) descriptions (see Fig. 11).

We may give a physical interpretation to the parameters of the Regge-pole analysis, and in so doing demonstrate that this interpretation is consistent with the assumptions of the DWBA analysis. In particular, the Regge-pole description suggests that for a very short time the two interacting nuclei might be considered to form a "quasimolecular" state with angular momentum l_0 = Reα. For a given internuclear distance R_{rot} the moment of inertia is $\mathscr{I} = \mu R_{rot}{}^2$, where μ is the reduced mass of the quasimolecular system. The rotational energy is then

$$E = \text{const} + \frac{\hbar^2}{2\mathscr{I}} l_0(l_0+1), \qquad (20)$$

and the moment of inertia may be determined by plotting the quantity $l_0(l_0+1)$ as a function of channel energy. This has been done for both the initial and final channels in Fig. 13. As is evident from the figure, Eq. (20) is valid to a satisfactory degree of accuracy. From the slope of the $l_0(l_0+1)$ vs E plot one obtains for both the initial and final channels

$$\frac{2\mathscr{I}}{\hbar^2} = 33.3 \text{ MeV}^{-1},$$

corresponding to R_{rot} = 8.3 fm and 8.6 fm for the entrance and exit channels, respectively. Such rotational separations are approximately equal to that *distance* where a radial cutoff starts to reduce the predicted DWBA total cross section (see Table VI). It should be pointed out that the concept of a "quasirotational" state is not essential to an understanding of the linear dependence of $l_0(l_0+1)$ on E shown in Fig. 13. It is sufficient that the reaction be peripheral so that $k^2 b^2$ = $l_0(l_0+1)$ (k is the wave number and b is the impact parameter for the two nuclei). The Regge-pole description contains this feature and thus provides a natural interpretation for the linear dependence with reasonable values for the internuclear distance R_{rot}.

A Regge pole is perhaps more properly interpreted[12,13] as a damped surface wave traveling around the nuclear surface. The damping con-
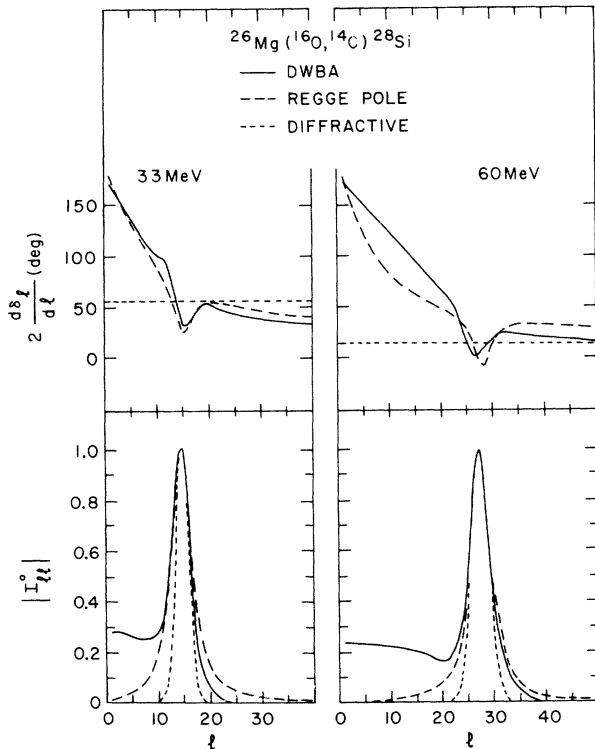
FIG. 11. Comparison of magnitudes and phase derivatives of the transfer amplitudes corresponding to DWBA, diffractive, and Regge-pole calculations which produce nearly identical angular distributions (see Fig. 12). Note that the transfer amplitudes are plotted as $|I_{ll}^0|$ without the factor $(2l+1)$ which usually is included in the DWBA amplitude (e.g., see Figs. 3 and 6 and Ref. 27). Thus, the Gaussian and Lorentzian forms of the diffractive and Regge amplitudes respectively are apparent and can be compared directly. The diffractive and Regge-pole predictions shown were obtained by a least squares fit to the angular shape predicted in the DWBA and shown with the experimental data in Fig. 1. The optimum fit diffractive and Regge-pole parameters are given in Table VIII. The comparison is made both at 33 MeV (left) and 60 MeV (right) incident energy.

stant in the angular direction, i.e., the "life angle" of the surface wave, is given by $(\mathrm{Im}\alpha)^{-1}$. For the calculations shown in Fig. 10 at incident energies ≤ 60 MeV, $\mathrm{Im}\alpha \approx 2.4$, which corresponds to a life angle of $24°$. The surface waves decay very rapidly ly, surviving less than a tenth of one revolution. This already has been stressed in Ref. 14, where the term "peripheral fly-off resonance" has been introduced to contrast with the more usual concept of orbiting. To reinforce this point the width of the "peripheral fly-off resonance" also may be calculated by the relation[12]

$$\tfrac{1}{2}\Gamma = \frac{\mathrm{Im}\alpha(E_0)\mathrm{Re}\alpha'(E_0)}{|\alpha'(E_0)|^2} \,. \tag{21}$$

Here a prime denotes differentation with respect

to the energy. Using Eq. (20) for $\mathrm{Re}\alpha$ and noting that for $E_{\mathrm{inc}} \leq 60$ MeV $\mathrm{Im}\alpha'(E) \approx 0$ (see Table VII) one obtains

$$\tfrac{1}{2}\Gamma = \frac{\mathrm{Im}\alpha(E_0)\hbar^2(2l_0+1)}{2s} \,. \tag{22}$$

For the value of $2s/\hbar^2 = 33.3$ MeV^{-1} and the value $\mathrm{Im}\alpha = 2.4$ we may estimate the width

$$\Gamma \approx 0.14(2l_0+1) \text{ MeV} \,.$$

The spacing of the resonances may be written as[40]

$$D = \frac{\Gamma}{2\mathrm{Im}\alpha} \tag{23}$$

or, for our special case,

$$D \approx 0.030(2l_0+1) \text{ MeV} \,.$$

At a laboratory energy of 40 MeV, $l_0 \approx 18$ and one obtains $\Gamma \approx 5.2$ MeV and a spacing of the resonances of $D \approx 1.1$ MeV. Therefore, as has been pointed out by Fuller,[40] one does not populate single isolated
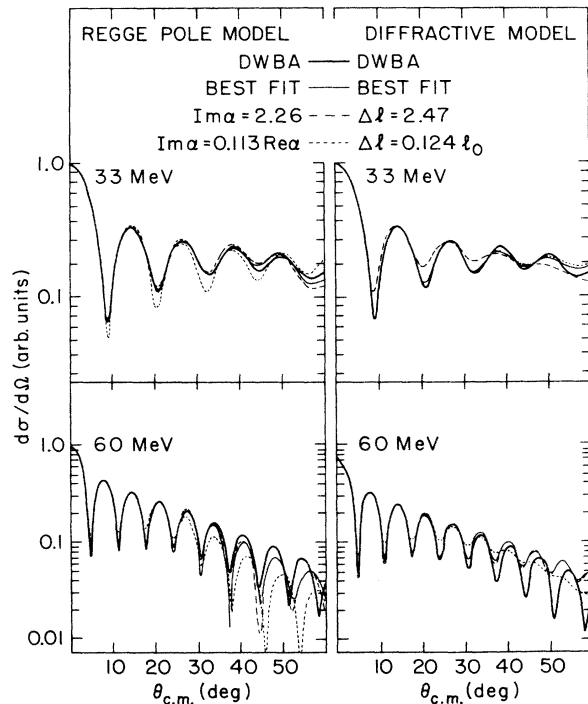
FIG. 12. Fits of DWBA calculations by Regge (left side) and diffraction (right side) parametrizations. The full curves are the DWBA calculations shown with the data in Fig. 1. The thin curves are best fits to the DWBA curves obtained by varying all three parameters. The dashed curves are obtained by keeping $\mathrm{Im}\alpha$ (left) or Δl (right) constant with energy. The dotted curves correspond to keeping $\mathrm{Im}\alpha/\mathrm{Re}\alpha$ (left) or $\Delta l/l_0$ (right) constant with energy. The parameters corresponding to the diffractive and Regge-pole calculations are given in Table VIII.
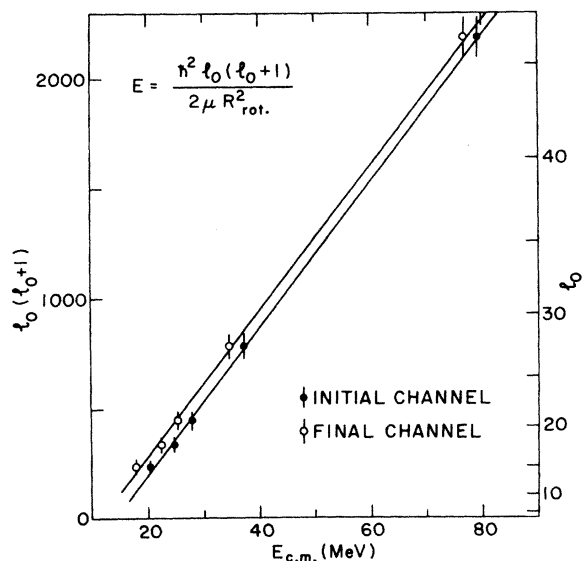
FIG. 13. Plot of $l_0(l_0+1)$ versus the center-of-mass energies of the initial and final channels. The values of l_0 as determined from $l_0 = \mathrm{Re}\,\alpha$ in the Regge-pole analysis of the angular shape have been used (see Table VII). Since the transition is well matched in l space, identical poles and therefore l_0's have been used for the entrance and exit channels. These values are nearly identical to the l_0's obtained in the DWBA analysis (see Table IV). The error flags indicated represent an uncertainty in l_0 of one unit of angular momentum.

resonances which would extend around the nucleus but instead several broad overlapping resonances. At 40 MeV laboratory energy their lifetime may be estimated to be $T \approx 1.3 \times 10^{-22}$ sec, which is of the order of magnitude of the time the nuclei take to fly past each other. Such a value is consistent with the direct reaction mechanism assumed in this analysis and in the DWBA description.

VI. SUMMARY

The oscillating shape of the $^{26}\mathrm{Mg}(^{16}\mathrm{O},\,^{14}\mathrm{C})^{28}\mathrm{Si}_{g.s.}$ angular distributions at 33, 40, 45, 60, and 128 MeV incident energy are reproduced by diffractive, Regge-pole, and DWBA analyses. The first two descriptions do not depend on detailed assumptions about the wave functions or the interactions involved. They are successful in describing the angular shape because of the peripheral nature of the reaction. A comparison of the reaction amplitudes obtained from the DWBA with the Gaussian and Lorentzian shapes of the diffraction and Regge models, respectively, shows that the angular dis-

tributions do not sensitively depend on the details of the transition amplitude but only on some average quantities like the position and the width of the l-space localization. Even a linear dependence of the phase shifts on angular momentum gives a good description of the present data. This indicates that the main reason for the occurrence of the strong oscillations in the present angular distributions is the diffraction due to the strong l-space localization. The effect of a phase nonlinear in l such as predicted in the DWBA analysis is a modulation of the amplitudes of the oscillations[15,39] which would be difficult to observe experimentally. The success of the Regge-pole formalism for such transfers stresses the importance of the peripheral distorted waves to the reaction dynamics. The parameters of such a "Regge-pole resonance" used to reproduce the transfer data are consistent with the l-space localization in the DWBA and diffractive analyses. The implied "life angle" of the peripheral resonance ($\approx 24°$) is much less than one revolution, i.e., it is consistent with the assumed direct reaction mechanism.

The sensitivity of the predicted DWBA angular shapes to the details of the absorptive potential suggests an energy dependent imaginary potential in the nuclear surface region. Such a potential removes much of the variation of the normalization between calculated and experimental cross sections with incident energy; however, the DWBA calculations yield the absolute cross section which are too small by more than two orders of magnitude at the lower energies. It is expected that recoil[23] and an enlarged configuration basis[34] would improve the agreement significantly. It is noted that second order processes have been suggested[41] to contribute significantly to the $^{26}\mathrm{Mg}(^{16}\mathrm{O},\,^{14}\mathrm{C})$ transition to the lowest 2^+ and 4^+ excited states of $^{28}\mathrm{Si}$. Similar processes also may contribute to the transition strength populating the $^{28}\mathrm{Si}$ ground state and might be an explanation for the energy dependence of the imaginary potential in the nuclear surface region which has to be introduced in a single step DWBA calculation.

†Summer visitor 1974. Permanent address: Max-Planck-Institut für Kernphysik, 69 Heidelberg, P. O.

Box 103980, Germany.

[1]See, e.g., *Proceedings of the Symposium on Heavy Ion Reactions and Many Particle Excitations* [J. Phys. (Paris) 32, C6 (1971)]; Proceedings of the Symposium on Heavy-Ion Transfer Reactions, Argonne, 1973 [ANL Report No. PHY-1973B (unpublished)]; *Proceedings of the International Conference on Reactions between Complex Nuclei, Nashville, Tennessee, 1974,* edited by R. L. Robinson, F. K. McGowan, J. B. Ball, and J. H. Hamilton (North-Holland, Amsterdam/American-Elsevier, New York, 1974), Vols. I & II; *Proceedings of the Symposium on Classical and Quantum Mechanical Aspects of Heavy Ion Collisions, Heidelberg, 1974,* edited by H. L. Harney, P. Braun-Munzinger, and C. K. Gelbke (Springer-Verlag, Berlin, 1975), Lecture Notes in Physics Series Vol. 33.

[2]See however, P. D. Bond, J. D. Garrett, O. Hansen, S. Kahana, M. J. LeVine, and A. Z. Schwarzschild, Phys. Lett. 47B, 231 (1973); U. C. Schlotthauer-Voos, H. G. Bohlen, V. von Oertzen, and R. Bock, Nucl. Phys. A180, 385 (1972).

[3]P. R. Christensen, O. Hansen, J. S. Larsen, D. Sinclair, and F. Videbaek, Phys. Lett. 45B, 107 (1973); and J. B. Ball, D. Sinclair, J. S. Larsen, O. Hansen, and F. Videbaek, *ibid.* 49B, 348 (1974); and (to be published).

[4]T. M. Cormier, E. R. Cosman, A. Sperduto, K. van Bibber, A. J. Lazzarini, A. Graue, H. E. Wegner, and J. D. Garrett, Bull. Am. Phys. Soc. 19, 46 (1974); and (to be published).

[5]D. Sinclair, Phys. Lett. 53B, 54 (1974).

[6]V. M. Strutinsky, Zh. Eksp. Teor. Fiz. 46, 2078 (1964) [Sov. Phys.—JETP 19, 1401 (1964)].

[7]A. Dar, Phys. Rev. 139, B1193 (1965); Nucl. Phys. 82, 354 (1966).

[8]W. E. Frahn and M. A. Sharaf, Nucl. Phys. A133, 593 (1969).

[9]K. Alder and D. Trautmann, Ann. Phys. (N. Y.) 66, 884 (1971).

[10]W. E. Frahn, in Lectures given at the Extended Seminar on Nuclear Physics, 1973, International Centre for Theoretical Physics, Trieste, Italy (unpublished).

[11]S. Kahana, P. D. Bond, and C. Chasman, Phys. Lett. 50B, 199 (1974); see also S. Kahana, in *Proceedings of the International Conference on Reactions between Complex Nuclei, Nashville, Tennessee, 1974* (see Ref. 1), Vol. II, p. 189.

[12]R. C. Fuller, Nucl. Phys. A216, 199 (1973).

[13]R. C. Fuller and Y. Avishai, Nucl. Phys. A222, 365 (1974).

[14]R. C. Fuller and O. Dragun, Phys. Rev. Lett. 32, 617 (1974).

[15]K. W. McVoy, in *Proceedings of the Symposium on Classical and Quantum Mechanical Aspects of Heavy Ion Collisions, Heidelberg, 1974* (see Ref. 1), p. 127.

[16]R. C. Fuller and K. W. McVoy, Phys. Lett. B55, 121 (1975).

[17]M. J. LeVine and H. A. Enge, Bull. Am. Phys. Soc. 15, 1688 (1970).

[18]J. B. Marion and F. C. Young, *Nuclear Reaction Analysis* (North-Holland, Amsterdam, 1968), pp. 41, 43.

[19]N. Austern, *Direct Nuclear Reaction Theories* (Wiley, New York, 1970).

[20]A. J. Baltz and S. Kahana, Phys. Rev. Lett. 29, 1267 (1962).

[21]F. Schmittroth, W. Tobocman, and A. A. Golestaneb, Phys. Rev. C 1, 377 (1970).

[22]J. S. Blair, R. M. DeVries, K. G. Nair, A. J. Baltz, and W. Reisdorf, Phys. Rev. C 10, 1856 (1974).

[23]B. F. Bayman, Phys. Rev. Lett. 32, 71 (1974).

[24]B. Nilsson, R. A. Broglia, S. Landowne, R. Liotta, and A. Winther, Phys. Lett. 47B, 189 (1973).

[25]P. D. Bond, J. D. Garrett, S. Kahana, M. J. LeVine, and A. Z. Schwarzschild, in *Proceedings of the International Conference on Reactions between Complex Nuclei, Nashville, Tennessee, 1974* (see Ref. 1), Vol. I, p. 54.

[26]M. J. LeVine, A. J. Baltz, P. D. Bond, J. D. Garrett, S. Kahana, and C. E. Thorn, Phys. Rev. C 10, 1602 (1974).

[27]J. D. Garrett, in *Proceedings of the Symposium on Classical and Quantum Mechanical Aspects of Heavy Ion Collisions, Heidelberg, 1974* (see Ref. 1), p. 59.

[28]A. J. Baltz, P. D. Bond, J. D. Garrett, and S. Kahana, Phys. Rev. C 12, 136 (1975).

[29]The particular parametrization of the surface transparent potentials incorporating a strongly absorbing Woods-Saxon potential in the nuclear interior together with a weak surface derivative absorptive term near the nuclear surface is given in Table II and is discussed in Refs. 25-28. Similar results probably could be obtained with a strongly absorbing potential of Woods-Saxon geometry having a very small diffusivity (see Ref. 28) similar to those used by other groups. See, e.g., M.-C. Lemaire, M. C. Mermaz, H. Sytark, and A. Cunsolo, Phys. Rev. C 10, 1103 (1974); W. Henning, D. G. Kovar, B. Zeidman, and J. R. Erskine, Phys. Rev. Lett. 32, 1015 (1974). The convenience of the parametrization used here is apparent when it becomes necessary to vary the absorption at the nuclear surface as a function of the channel energy.

[30]I. Tserruya, W. Bohne, P. Braun-Munzinger, C. K. Gelbke, W. Grochulski, H. L. Harney, and J. Kuzminski, Nucl. Phys. A242, 345 (1975); see also P. D. Bond *et al.* in Ref. 2.

[31]C. Chasman, S. Kahana, and M. J. Schneider, Phys. Rev. Lett. 31, 1074 (1973).

[32]J. B. Ball, O. Hansen, J. S. Larsen, D. Sinclair, and F. Videbaek, Nucl. Phys. A244, 341 (1975).

[33]J. D. Garrett, H. E. Wegner, T. M. Cormier, E. R. Cosman, O. Hansen, and A. J. Lazzarini, Phys. Rev. C12, 489 (1975).

[34]J. Bang, F. A. Gareev, and B. S. Nilsson, in *Proceedings of the International Conference on Reactions between Complex Nuclei, Nashville, Tennessee, 1974* (see Ref. 1), Vol. I, p. 55; and J. Bang, C. H. Dasso, F. A. Careev, and B. S. Nilsson, Phys. Lett. 53B, 143 (1974).

[35]R. Rost and N. Austern, Phys. Rev. 120, 1375 (1960).

[36]N. Austern, Ann. Phys. (N. Y.) 15, 299 (1961).

[37]It is emphasized that the use of a cutoff on the radial interaction is a computational technique— not a physical one. It does not completely remove the effects of the nuclear interior. It does indicate, however, at what radii large contributions to the calculated cross sections are obtained.

[38]Corresponds to cutoff radii where σ_{total} is 50% of the value for no cutoff in the radial integration. The errors given correspond to 90% and 10% of the zero

cutoff cross section.

[39]W. A. Friedman, K. W. McVoy, and G. W. T. Shuy, Phys. Rev. Lett. <u>33</u>, 308 (1974).

[40]R. C. Fuller, as quoted in Ref. 15.

[41]B. Sørensen, in *Proceedings of the International Conference on Reactions between Complex Nuclei, Nashville, Tennessee, 1974* (see Ref. 1), Vol. I, p. 50; Phys. Lett. <u>53B</u>, 285 (1974).